Monitoring the Photocleaving Dynamics of Colloidal MicroRNA–Functionalized Gold Nanoparticles Using Second Harmonic Generation

ARTICLE *in* LANGMUIR · AUGUST 2015

Impact Factor: 4.46 · DOI: 10.1021/acs.langmuir.5b02199

5 AUTHORS, INCLUDING:

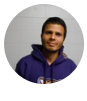

Raju Ram Kumal

Louisiana State University

4 PUBLICATIONS **3** CITATIONS

Langmuir

Article

pubs.acs.org/Langmuir

Monitoring the Photocleaving Dynamics of Colloidal MicroRNA-Functionalized Gold Nanoparticles Using Second Harmonic Generation

Raju R. Kumal,[†] Corey R. Landry,[‡] Mohammad Abu-Laban,[‡] Daniel J. Hayes,[‡] and Louis H. Haber*[,†]

[†]Department of Chemistry and [‡]Department of Biological, Agricultural Engineering, Louisiana State University, Baton Rouge, Louisiana 70803, United States

ABSTRACT: Photoactivated drug delivery systems using gold nanoparticles provide the promise of spatiotemporal control of delivery that is crucial for applications ranging from regenerative medicine to cancer therapy. In this study, we use second harmonic generation (SHG) spectroscopy to monitor the light-activated controlled release of oligonucleotides from the surface of colloidal gold nanoparticles. MicroRNA is functionalized to spherical gold nanoparticles using a nitrobenzyl linker that undergoes photocleaving upon ultraviolet irradiation. The SHG signal generated from the colloidal nanoparticle sample is shown to be a sensitive probe for monitoring the photocleaving dynamics in real time. The photocleaving irradiation wavelength is scanned to show maximum efficiency on resonance at 365 nm, and the kinetics are investigated at varying irradiation powers to demonstrate that the nitrobenzyl photocleaving is a one-photon process. Additional characterization methods including electrophoretic mobility measurements, extinction spectroscopy, and fluorimetry are used to verify the SHG results, leading to a better understanding of the photocleaving dynamics for this model oligonucleotide therapeutic delivery system.

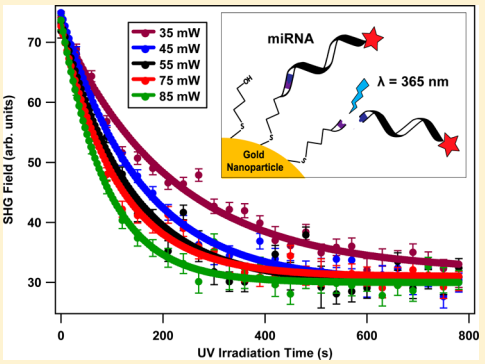

INTRODUCTION

Short oligonucleotides including small interfering RNA (siRNA) and microRNA (miRNA) are involved in the post-translational control of gene expression and have become increasingly important in basic and applied biology.[1−6] Because systemically administered siRNA and miRNA are rapidly degraded by RNases in the bloodstream before reaching their cellular targets, methods of protecting and delivering these oligonucleotides are important to the development of RNA-based therapeutics.[7−10] Thiolation of synthetic oligonucleotide strands and attachment to metal nanoparticles has become an important method to protect the oligonucleotide from enzymatic degradation and to facilitate transport into the cell.[11,12] Our previous work has demonstrated that short nucleotide strands of antisense DNA[13] and osteogenic miRNA-148b[14] are able to be attached to silver nanoparticles through thiol functionalization and then transported into mammalian cells, altering their fate after being released from the particle by photoactivation. Light activation presents a method with a greater potential for spatiotemporally controlled release than alternate methods based on chemical stimuli, pH, or ionic strength.[14−18]

The unique optical properties of gold nanoparticles (GNPs), especially their activity in the visible and near-infrared regions, along with their biocompatibility and ease of synthesis, enable a number of applications including molecular sensing, labeling, drug delivery, and photothermal cancer treatment.[15−19] The optical properties of GNPs are derived from the surface plasmon resonances, which are characterized by the coherent oscillation of free electrons under incident light.[20−23] The plasmon resonances can cause significant optical field enhancements leading to processes such as surface enhanced Raman spectroscopy (SERS),[24,25] surface enhanced fluorescence,[26,27] and plasmon-exciton polariton resonant coupling.[28] Gold nanoparticles having various geometries such as nanorods, nanocages, and nanoshells are attractive nanomaterials for optical contrast enhancement agents, cancer diagnosis, and therapeutics.[29−31] Recent in vivo studies of oligonucleotide-functionalized GNPs have demonstrated their powerful ability for cancer gene therapy through controlled release.[32,33] GNPs can be functionalized with miRNA using the same thiolization method as silver nanoparticles and many other metallic nanoparticles.[13,14] To date, several groups have investigated light-activated nucleic acid delivery using GNPs to demonstrate the controlled release of DNA,[16,17] the selective release of multiple DNAs,[18] and light-activated gene silencing.[15]

Here, we report the use of nonlinear spectroscopy to probe the nanoparticle surface during the process of oligonucleotide photorelease. Nonlinear laser spectroscopies such as second harmonic generation (SHG) and sum frequency generation are powerful, noninvasive, surface-sensitive techniques that are useful for the investigation of colloidal nanoparticles.[28,34−36] In

Received: June 15, 2015
Revised: August 21, 2015

DOI: 10.1021/acs.langmuir.5b02199
Langmuir XXXX, XXX, XXX−XXX

SHG spectroscopy, two incident photons of frequency ω add coherently to generate a photon of frequency 2ω. SHG is dipole forbidden in bulk media with inversion symmetry, but it can be generated from the surface and interfaces of nanoparticles where the inversion symmetry is broken.[37−39] The release of highly negatively charged miRNA from the surface of GNPs is an ideal candidate for SHG spectroscopy investigations. The SHG signal from this charged interface has two components given by the second-order susceptibility $\chi^{(2)}$, which is based on the two-photon spectroscopy, and the third-order susceptibility $\chi^{(3)}$, which is based on the electrostatic potential from the nanoparticle surface.[40−43] The SHG electric field E_{SHG} is proportional to the square root of the SHG signal and is given by

$$E_{SHG} = \chi^{(2)} E_\omega E_\omega + \chi^{(3)} E_\omega E_\omega \Phi_0 \quad (1)$$

where E_ω is the incident electric field of the fundamental laser at frequency ω and Φ_0 is the electrostatic surface potential. The $\chi^{(2)}$ term can be sensitive to any chemical change on the nanoparticle surface that causes a spectroscopic change at either ω or 2ω. The $\chi^{(3)}$ term depends on the net polarization of bulk molecules in the solvent, which are induced by the electric field of the nanoparticle surface.[44,45]

In this study, we demonstrate the applicability of SHG spectroscopy to light-activated gene delivery by measuring the wavelength and power dependence of the kinetics associated with miRNA release from GNPs using nitrobenzyl photocleavable (PC) chemistry. The experimental setup uses a probe laser at 800 nm to generate SHG signals for real-time monitoring of the miRNA photorelease from the GNP surface. A second laser is used to induce the photocleaving under varying wavelengths and powers. GNPs of 68 nm diameter are functionalized by a synthetic miRNA-148b that has been thiolated and modified with an ultraviolet-active nitrobenzyl photocleavable group,[14,46] as shown schematically in Figure 1. SHG measurements as a function of irradiation time using different photocleaving laser wavelengths are conducted and compared to corresponding fluorescence quantification measurements and extinction spectra to investigate photocleaving efficiencies. Additionally, analysis of the photocleaving dynamics are monitored using time-dependent SHG measurements under different ultraviolet (UV) irradiation powers to better understand the kinetics of the photocleaving process.

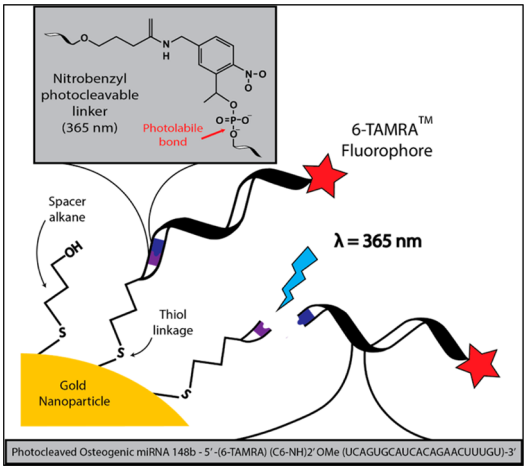

Figure 1. Schematic representation of the PC-miRNA-148b functionalized gold nanoparticle attached with fluorophore 6-TAMRA. The nitrobenzyl photocleavable group, between the spacer linker and the oligonucleotide, absorbs UV radiation centered near 365 nm to release the miRNA from the surface of the gold nanoparticle.

SYNTHESIS AND CHARACTERIZATION OF GOLD NANOPARTICLES

The colloidal gold nanoparticle sample of 68 nm diameter is prepared using a seeded-growth method where citrate is first used as a reducing agent and capping agent for the gold nanoparticle seeds followed by the addition of a stronger reducing agent, hydroquinone, to produce larger GNPs with low polydispersity. During the gold nanoparticle seed synthesis, 900 μL of 34 mM sodium citrate is added to 30 mL of 290 μM gold chloride in ultrapure water under boiling conditions with vigorous stirring. The solution changes color to a bright red after 10 min and is then cooled to room temperature. In the second step, 150 μL of the seed solution is added to 2.9 mM of gold chloride in 10 mL of ultrapure water, followed by the addition of 100 μL of 0.03 M hydroquinone and 22 μL of 34 mM sodium citrate. The solution is left to stir at room temperature for 60 min to produce the 68 nm colloidal gold nanoparticles.

The surface of the gold nanoparticles are functionalized with fluorophore-labeled miRNA via a "salt-aging" technique as described previously.[14] Here, 2.5 μL of 0.8 μg/μL of the miRNA-148b (PC-miR-148b) modified with the thiolated photocleavable nitrobenzyl group and labeled with a 6-TAMRA fluorophore group is added to 1 mL of the gold nanoparticles at a concentration of 8.25×10^9 nanoparticles/mL. The mixed samples are left to incubate for 24 h under gentle agitation conditions. Following the incubation period, 10 μL of 0.035 M sodium dodecyl sulfate (SDS) solution and 20 μL of 0.01 M phosphate buffer saline solution (PBS) solution are added to each sample. After an additional 3 h of incubation, a 10 μL solution of 2 M tris(hydroxymethyl) aminomethane (Tris) and 2 M NaCl is added three times, with 3 h of incubation between each salting step. The miRNA-functionalized nanoparticles are purified via centrifugation three consecutive times at 7000 rpm for 20 min each. During the first two centrifugation cycles, the precipitate obtained from 1 mL of sample is resuspended in 1 mL of solution containing 0.035 M SDS, 0.1 M Tris, 0.103 M NaCl, and 0.0005 M disodium diphosphate, and finally in 1 mL of deionized water after the third centrifugation.

The gold nanoparticles are characterized using transmission electron microscopy (TEM), dynamic light scattering, extinction spectroscopy, and zeta potential measurements. The average nanoparticle diameter is determined to be 68 ± 7 nm from TEM measurements, with representative TEM images shown in Figure 2a. Figure 2b shows TEM images of GNPs after functionalization with miRNA, where a very thin layer of approximately 2 nm in thickness is observed around the nanoparticles, showing the added functionalized miRNA. Figure 3 displays the experimental extinction spectrum of the 68 nm GNPs in water (red line) with a localized surface plasmon peak centered on 543 nm, compared to the best fit from Mie theory (dashed gray line) at a concentration of 8.25×10^9 nanoparticles/mL. Dynamic light scattering measurements determine the hydrodynamic diameter of the GNP sample to be 68 ± 15 nm, in agreement with the TEM and extinction spectroscopy results. The hydrodynamic diameter of the GNPs after functionalizing with miRNA increases to 140 ± 20 nm, due to the attached miRNA in solution.

DOI: 10.1021/acs.langmuir.5b02199
Langmuir XXXX, XXX, XXX−XXX

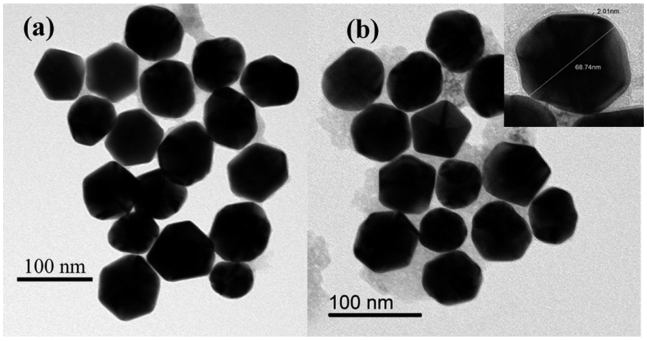

Figure 2. Representative TEM images of (a) gold nanoparticles and (b) gold nanoparticles functionalized with PC-miRNA-148b.

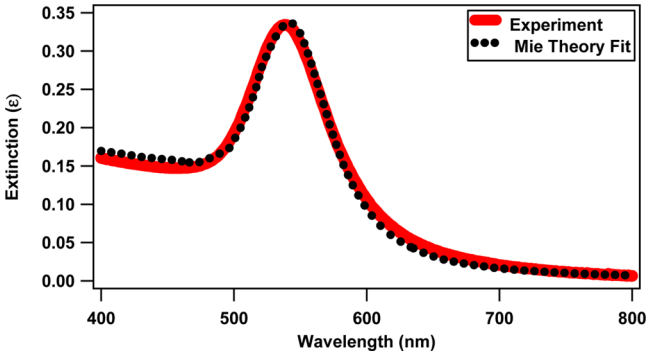

Figure 3. Extinction spectrum of the 68 nm colloidal gold nanoparticle sample in water (red line) compared with the best fit from Mie theory (dotted black line).

The zeta potential of the colloidal GNP sample before and after functionalization with miRNA is obtained from electrophoretic mobility measurements using the Huckel approximation.[47] The electrophoretic mobility for the GNPs and the GNPs functionalized with miRNA is shown in Figure 4. The

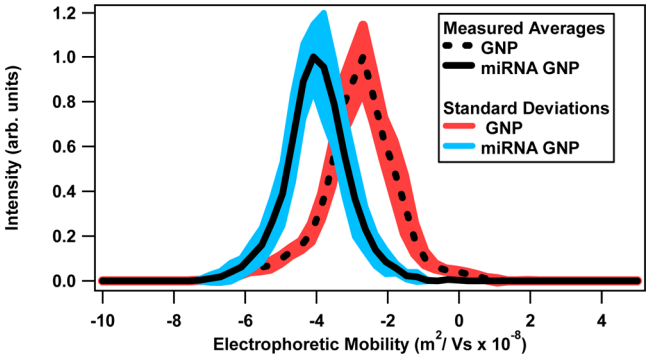

Figure 4. Electrophoretic mobility plot of gold nanoparticles and miRNA-functionalized gold nanoparticles showing the measured averages (dashed and solid black lines, respectively) and corresponding standard deviations (red and blue areas, respectively).

electrophoretic mobility of GNPs is measured to be $(-2.65 \pm 0.8) \times 10^{-8}$ $m^2/(V\ s)$ with a corresponding zeta potential of -50 ± 17 mV. The electrophoretic mobility of miRNA-functionalized GNPs is measured to be $(-3.98 \pm 0.9) \times 10^{-8}$ $m^2/(V\ s)$ with a corresponding zeta potential of -76 ± 18 mV, where the highly charged miRNA attached to the surface in aqueous solution increases the negative zeta potential.

EXPERIMENTAL SETUP

The experimental setup for the second harmonic generation studies, shown schematically in Figure 5, is modified from a

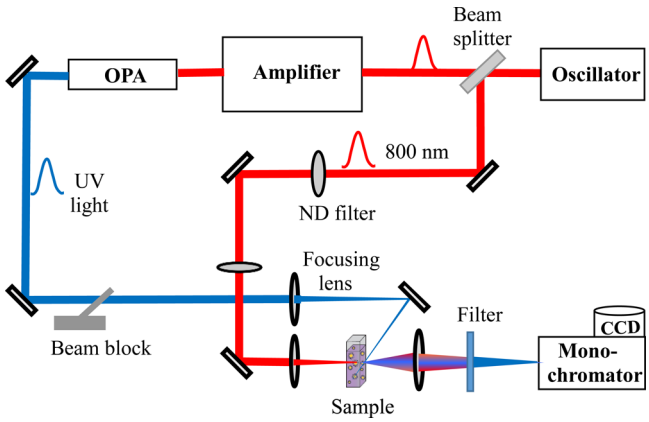

Figure 5. Experimental setup showing the UV beam (blue) and 800 nm probe (red) beam, which are focused to the colloidal nanoparticle sample in a 1 cm quartz cuvette, with the SHG signal detected using a spectroscopy CCD detector.

previously reported version.[28,45] The setup uses a titanium:sapphire oscillator laser, a titanium:sapphire amplifier laser, an optical parametric amplifier (OPA) laser, an optical setup, and a high-sensitivity CCD spectroscopy detector. The oscillator laser operates at a center wavelength of 800 nm with 75 fs pulses at a repetition rate of 80 MHz and an average power of 2.5 W. A beamsplitter separates the oscillator laser beam into one path that is used as the probe laser for the SHG measurements and another path that is used to seed the amplifier. A portion of the amplifier laser is sent through the OPA to generate the tunable UV or visible wavelengths with 100 fs pulses at a repetition rate of 10 kHz. The 800 nm probe laser beam for SHG measurements is attenuated to an average power of 790 mW and focused to the 1.5 mL colloidal sample, which is contained in a 1 cm by 1 cm quartz cuvette at a concentration of 8.25×10^9 nanoparticles/mL in water with the SHG collected in the forward direction. The wavelength-tunable visible or UV beam for photoactivation is directed to the nanoparticle sample at 90° with respect to the 800 nm beam. The SHG from the nanoparticle sample is measured as a function of the UV laser irradiation time for investigating photocleaving reaction dynamics from the miRNA-functionalized GNPs. A beam block opens and shuts on the photocleaving UV beam every 30 s in synchronization with an automated file-saving program so that the SHG can be measured in real time to monitor the photoactivated drug-delivery reaction. A variable neutral density filter is used to control the power of the UV laser. Automated stirring is initiated during the UV laser irradiation and is stopped when the UV laser is blocked for stable SHG measurements, which are collected at multiple 1 s acquisitions for statistical analysis.

RESULTS AND DISCUSSION

The light-activated controlled release of oligonucleotides from the surface of gold nanoparticles is monitored in real time using second harmonic generation. Representative SHG spectra of the GNPs and the miRNA-functionalized GNPs are shown in Figure 6a under the same 800 nm laser conditions and nanoparticle concentrations. The SHG peak is centered at 400

DOI: 10.1021/acs.langmuir.5b02199
Langmuir XXXX, XXX, XXX−XXX

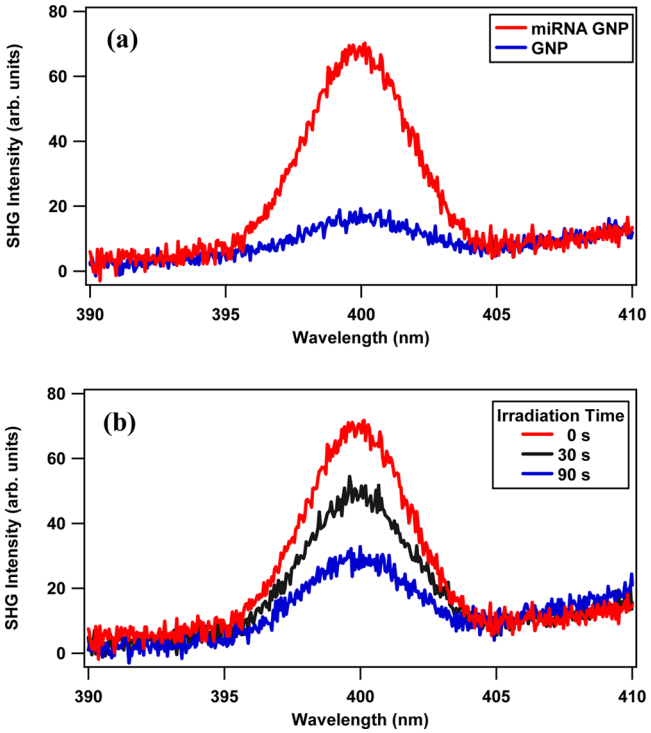

Figure 6. (a) SHG spectrum of a colloidal miRNA-functionalized gold nanoparticle sample compared with an SHG spectrum of gold nanoparticles only. (b) SHG spectra of an miRNA-functionalized colloidal gold nanoparticle sample after different UV irradiation times using 365 nm with 85 mW average power. The probe laser is fixed at 800 nm.

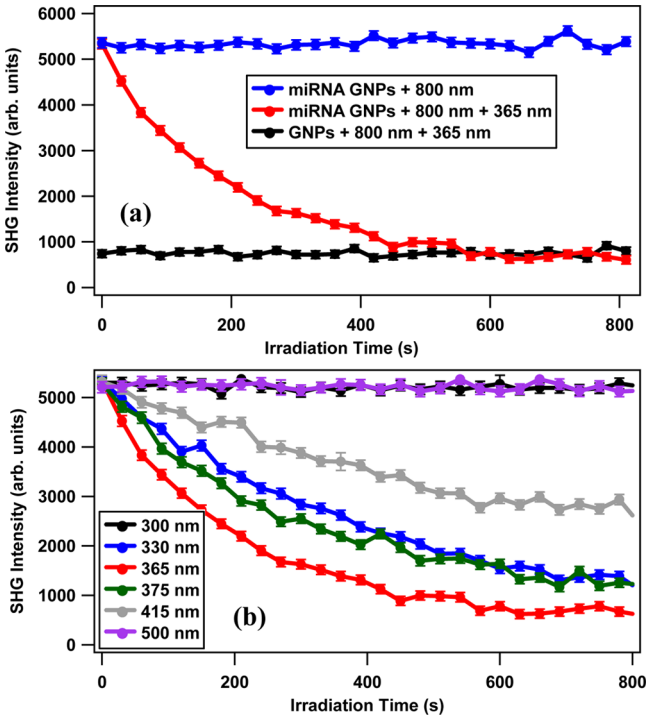

Figure 7. (a) The SHG signal remains constant in time for both the miRNA-functionalized GNPs using the 800 nm probe laser only (blue data) and the GNPs using the 800 nm probe and the UV laser at 365 nm (black data). The SHG decreases as a function of time when the miRNA-functionalized GNPs are irradiated with the UV laser at 365 nm (red data). (b) Time-dependent SHG measurements show the photocleaving dynamics of miRNA from the surface of gold nanoparticles using different UV and visible laser wavelengths at 20 mW average power.

nm with a full width half-maximum of 4.5 nm. The slight rise in signal at longer wavelengths is due to the two-photon fluorescence from the GNPs. The larger SHG signal from the miRNA-functionalized GNP sample compared to the GNP sample arises primarily as a consequence of the highly charged miRNA leading to a higher electrostatic surface potential magnitude and a larger $\chi^{(3)}$ term in eq 1, although some added contribution may also result from an increased $\chi^{(2)}$ term. The 6-TAMRA fluorophore label attached to the miRNA is chosen for corresponding fluorescence quantization measurements, while having minimal absorption at either 800 or 400 nm, where no added fluorescence is observed in the SHG spectra, so the fluorophore is expected to have negligible SHG contribution. Figure 6b displays the SHG spectra of the miRNA-functionalized GNPs exposed to different UV irradiation times of 0, 30, and 90 s using 365 nm at 85 mW. As the UV irradiation time increases, the SHG intensity decreases and asymptotically approaches a minimum value. The decrease in SHG intensity as a function of UV laser irradiation time is due to the change in the surface structure and surface charge leading to a change in the corresponding $\chi^{(2)}$ and $\chi^{(3)}$ terms upon photocleaving. The change in the $\chi^{(3)}$ term is expected to be the dominant contribution to the change in the SHG signal due to the loss of the highly charged miRNA upon photocleaving.

Figure 7a displays results from control experiments that show the SHG signal from GNPs and miRNA-functionalized GNPs as a function of time. The SHG signal for the miRNA-functionalized GNPs is shown to remain constant over time when using the 800 nm probe laser only (blue data points). Additionally, the SHG signal from the GNPs is shown to remain constant over time when using both the 800 nm probe laser and the UV laser at 365 nm and 20 mW average power (black data points), while maintaining a much lower SHG signal than the miRNA-functionalized GNPs. However, the SHG signal from the miRNA-functionalized GNPs decreases as a function of time and asymptotically approaches a minimum value when using both the 800 nm probe laser and the UV laser at 365 nm and 20 mW average power (red data points) due to the photocleaving dynamics. The asymptotic minimum value of the miRNA-functionalized GNPs after UV irradiation is approximately equal to the SHG signal of the GNPs, indicating that the miRNA-functionalized GNPs have roughly the same SHG signal as the GNPs after photocleaving is complete. This real-time monitoring of photocleaving dynamics is investigated under varying UV laser wavelengths and powers, and the photocleaving results are verified using extinction spectroscopy and fluorimetry measurements.

Figure 7b shows a wavelength-dependent study on the photocleaving dynamics of miRNA from the nanoparticle surface. When the sample is irradiated with the UV laser at 365 nm, which is on resonance with the PC linker, there is a fast decay of the SHG signal, corresponding to a fast rate of photocleaving and a large release of miRNA. The decay rate of the SHG signal decreases when the UV wavelength is off resonance compared to the PC linker, resulting in a slower rate of photocleaving and nucleotides release. The time-dependent SHG intensity under the UV irradiation wavelengths of 330, 375, and 415 nm results in slower rates of photocleaving in comparison to the 365 nm results, while irradiation at 500 and 300 nm does not produce any measurable photocleaving. The

DOI: 10.1021/acs.langmuir.5b02199
Langmuir XXXX, XXX, XXX−XXX

UV laser power is kept constant at 20 mW for direct comparison of the photocleaving rate at all of these wavelengths.

In order to quantify the photocleaving dynamics, a simple model is described. SHG is understood to be a coherent process from the surface of each individual colloidal nanoparticle, while the overall SHG signal is the incoherent sum of the SHG signal from each nanoparticle in the probe laser focus such that the SHG signal is linearly proportional to the nanoparticle concentration.[34,38] Therefore, using the results from Figure 7(a), the SHG electric field can be expressed using the equation $E_{SHG} = A + B[C]$, where A is an offset that includes background signal and the SHG from GNPs, $[C]$ is the cumulative concentration of attached miRNA on the GNP surface, and B is a proportionality constant. If we assume a single UV photon causes photocleaving from a single miRNA attached to the GNP surface with an associated equilibrium constant k, then the change in $[C]$ with respect to time $d[C]/dt$ is equal to $-k[C][h\nu]$, where $[h\nu]$ is the concentration or intensity of UV light. Under constant UV irradiation intensity, the time dependence of $[C]$ should follow an exponential decay given by $[C](t) = [C]_0 e^{-k't}$, where $[C]_0$ is the initial concentration of attached miRNA on the GNP surface and $k' = k[h\nu]$. Notice that the pseudo first-order rate constant k' is linearly proportional to the UV light intensity. Under this simple model, assuming the photocleaving occurs through a one-photon process, the SHG electric field, which is proportional to the square root of the SHG signal, is expected to decay exponentially as a function of UV irradiation time, with a rate constant that is linearly proportional to the UV laser power.

In order to test the accuracy of this model, the kinetics of the photocleaving process for miRNA-functionalized GNPs are studied using different UV laser powers centered at 365 nm. The measured time-dependent SHG electric field from the colloidal miRNA-functionalized GNP sample under varying UV laser powers is shown in Figure 8a. Each set of results is fit to a pseudo first-order exponential decay, as explained above, for UV laser powers of 35 mW, 45 mW, 55 mW, 75 mW, and 85 mW, respectively, to obtain the rate constants k' of $(4.6 \pm 0.4) \times 10^{-3}$ s^{-1}, $(6.4 \pm 0.4) \times 10^{-3}$ s^{-1}, $(7.6 \pm 0.8) \times 10^{-3}$ s^{-1}, $(9.7 \pm 0.6) \times 10^{-3}$ s^{-1}, and $(11.2 \pm 0.7) \times 10^{-3}$ s^{-1}, respectively. Figure 8b displays these measured rate constants as a function of UV laser power. The linear best fit is given by a slope of $(1.26 \pm 0.07) \times 10^{-4}$ s^{-1} mW^{-1} and a y-intercept of $(4.7 \pm 4.5) \times 10^{-4}$ s^{-1} and is in excellent agreement with the data, verifying that the photocleaving associated with the miRNA-functionalized GNPs is a one-photon process.

The laser-assisted controlled release of miRNA from the surface of GNPs is further analyzed using extinction spectroscopy measurements. Figure 9 shows a significant shift in plasmon peak of the GNPs from 543 to 553 nm after functionalization with nucleotides. The extinction spectra is blueshifted after UV laser irradiation of the sample compared to the original miRNA-functionalized GNP sample. These results further indicate that the oligonucleotides are releasing from the surface of GNP upon the UV laser irradiation. Analysis of these measurements demonstrates that the extinction spectrum of colloidal GNPs closely matches the extinction spectrum of the miRNA functionalized GNP sample after irradiation at 20 mW of 365 nm for 13 min, with the plasmon peak blueshifting back to 543 nm. At longer UV irradiation wavelengths of 375 and 390 nm, under 20 mW for 13 min there is less blueshifting in

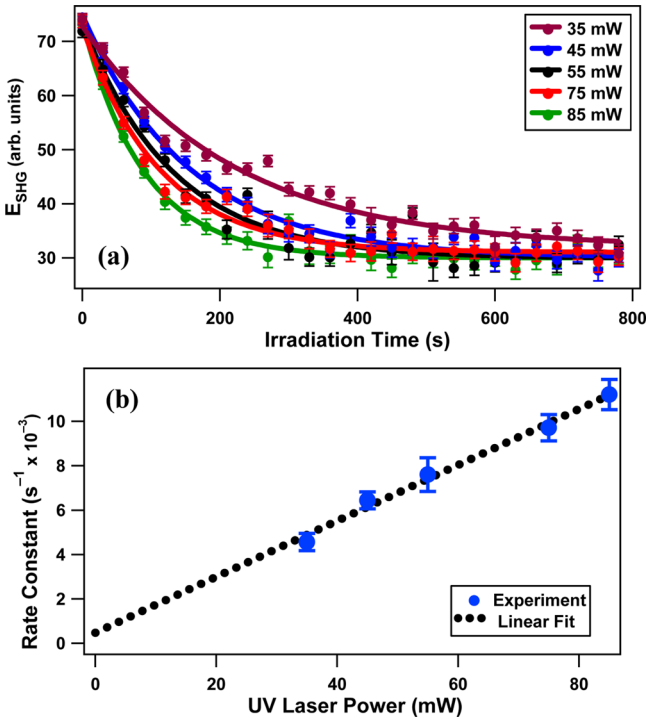

Figure 8. (a) Measured SHG electric field from miRNA-functionalized GNPs as a function of irradiation time with 365 nm at different UV laser average powers with corresponding exponential fits. (b) The obtained rate constants are plotted as a function of UV laser power. The linear variation as a function of laser power indicates a one-photon process.

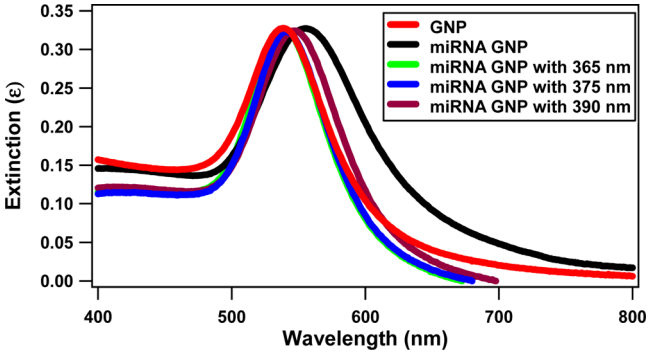

Figure 9. Extinction spectra of colloidal miRNA-functionalized gold nanoparticles after irradiating at different UV laser wavelengths. The extinction spectrum of the miRNA- functionalized GNPs is red-shifted with respect to the spectrum of GNPs only. After photocleavage with UV laser irradiation, all spectra are blueshifted compared to the miRNA-functionalized GNPs.

the extinction spectra compared to the miRNA-GNPs, going back to plasmon peaks of 545 and 548 nm, respectively, indicating incomplete photocleaving of the miRNA from the gold nanoparticle surface. However, the extinction coefficients at 800 and 400 nm change only slightly upon photocleaving, giving more evidence that the large change in the SHG signal is predominantly caused by the change in the electrostatic surface potential.

The amount of miRNA released from the surface of the nanoparticles is quantified using fluorescence measurements. For comparison, the concentration of miRNA molecules on the surface of the GNPs are first quantified using fluorescent-plate

DOI: 10.1021/acs.langmuir.5b02199
Langmuir XXXX, XXX, XXX−XXX

readings after chemical detachment of the miRNA. A volume of 10 μL of 65 mM of dithiothreitol (DTT) is added to 1 mL of the gold nanoparticles to reduce the miRNA, followed by agitation and 20 min of incubation at 37 °C for complete chemical cleavage of the oligonucleotides. The samples are then centrifuged at 7000 rpm, and three separate 100 uL aliquots of the supernatant are transferred to a 96-well plate for each sample. The concentration is then determined from a constructed standardized curve of the 6-TAMRA fluorophore group that is attached to the end of the miRNA.[14] The oligonucleotide coverage for nanoparticles is determined to be 92 ± 21 oligo/nanoparticle, yielding a surface density of (6.30 ± 1.48) × 10^{-3} oligo/nm^2. The fluorescent signal after DTT reduction and after irradiation with 20 mW average power for the different laser wavelengths of 365, 375, 390, and 500 nm, respectively, for 13 min is shown in Figure 10. Photocleaving is

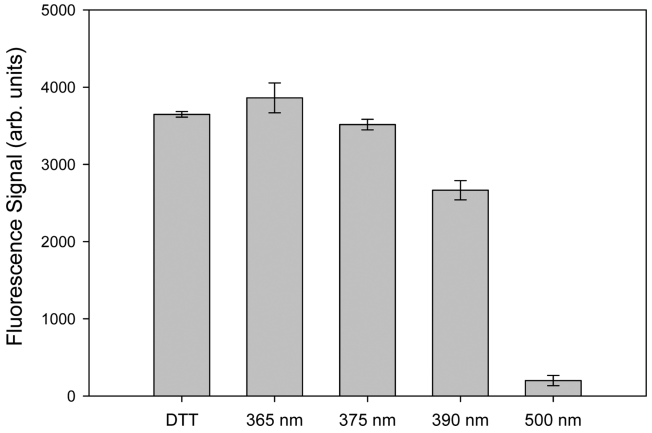

Figure 10. Fluorescence measurements of the supernatants of the miRNA-functionalized GNPs after chemical reduction with DTT and after 13 min of irradiation using 20 mW of 365, 375, 390, and 500 nm wavelengths, respectively.

shown to be most efficient at 365 nm on resonance with the nitrobenyl group, in agreement with the time-dependent SHG measurements. The corresponding extinction spectroscopy and fluorimetry measurements all agree with the general description provided by the SHG results, demonstrating a consistent interpretation of the photoactivated controlled release of oligonucleotides from the gold nanoparticle surface. Future research will work to investigate the role of plasmon enchancement on the photocleaving kinetics and extend the photocleaving wavelength to near-infrared energies for improved drug-delivery applications.

CONCLUSION

SHG is used to monitor the photoactivated controlled release of miRNA from the surface of colloidal gold nanoparticles. The SHG signal is seen to significantly decrease as a function of UV laser irradiation time, with larger photocleaving rates occurring at higher UV laser powers on resonance with the nitrobenzyl linker, according to a single-photon photocleaving process. The photocleaving dynamics are in excellent agreement with a model using a pseudo first-order rate equation. Corresponding extinction spectroscopy shows a redshift in the plasmon resonance peak after functionalizing the GNPs with miRNA and a blueshift after illumination with the UV laser, supporting the interpretation from the time-dependent SHG results. Fluorescent measurements also indicate that the miRNA is completely removed following UV laser irradiation. These results demonstrate the successful application of sensitive real-time measurements of photoactivated drug delivery using a model system of colloidal miRNA-functionalized gold nanoparticles in water.

MATERIALS AND METHODS

Chemicals and Reagents. For the synthesis of gold nanoparticles, high purity chemicals were purchased from Sigma-Aldrich, including gold(III) chloride hydrate (99.999%), sodium citrate dihydrate (≥99%) and hydroquinone (≥99%). Ultrapure water having resistivity of >18.2 MΩ was used during the synthesis and spectroscopic measurements. Custom thiol-functionalized miRNA-148b was purchased from Trilink Bio Technologies. The PBS solution, sodium chloride solid, and dithiothreitol were purchased from Sigma-Aldrich. Diethylpyrocarbonate (DEPC) water was purchased from Ambion, sodium dodecyl sulfate (SDS) from VWR, and tris(hydroxymethyl) aminomethane from Amresco.

Characterization of Gold Nanoparticles. The dynamic light scattering and electrophoretic mobilities of the colloidal gold nanoparticle samples were obtained using a Malvern Zetasizer (Nano series, Malvern Instruments Inc., UK). TEM images of nanoparticles before and after functionalization with miRNA were obtained using a high resolution JEOL JEM-2011 scanning TEM equipped with a Gatan SC1000 CCD camera and an EDAX EDS. Extinction measurements were acquired using a PerkinElmer Lambda 35 UV/Vis spectrophotometer.

Second Harmonic Generation Setup. The ultrafast laser systems used in this study include a Chameleon oscillator laser, a Legend Elite amplifier laser, and a TOPAS tunable optical parametric amplifier, which were all purchased from Coherent Inc. The signal detection was achieved using a spectrograph/monochromator (Acton SP2300) and CCD detector (PIXIS 400) purchased from Princeton Instruments.

PC-miR-148b Quantification. Oligonucleotide coverage of the gold nanoparticles was quantified using fluorescence spectroscopy and inductively coupled plasma optical emission spectroscopy (ICP-OES) measurements. PC-miR-148b oligonucleotides from the surface of gold nanoparticles were cleaved using 1% DTT and the tunable laser irradiation as mentioned above. After centrifugation, the supernatant was quantified with fluorimetry using a Wallac VICTOR2 V1420-040 Multilabel Counter (PerkinElmer, Boston, MA, USA) at excitation and emission wavelengths of 531 and 572 nm, respectively. The concentration of oligonucleotides was calculated using a standardized curve over various concentrations of PC-miR-148b. The gold nanoparticle content was quantified using ICP-OES (Varian, Palo Alto, CA, USA) after dissolving in 1.6 M nitric acid.

AUTHOR INFORMATION

Corresponding Author

*E-mail: lhaber@lsu.edu; phone: (225) 578-7965.

Notes

The authors declare no competing financial interest.

ACKNOWLEDGMENTS

Generous financial support for this work was provided by Louisiana State University, the National Science Foundation (CBET-1254281), and the National Institutes of Health (RDE024790A). The authors acknowledge Tony Karam and Dr. Zhenyu Zhang for many valuable discussions. We are also grateful to Dr. Raphael Cueto for his help with dynamic light scattering and zeta potential measurements and to Ying Xiao for her help with transmission electron microscopy.

DOI: 10.1021/acs.langmuir.5b02199
Langmuir XXXX, XXX, XXX−XXX

REFERENCES

(1) Davis, M. E.; Zuckerman, J. E.; Choi, C. H. J.; Seligson, D.; Tolcher, A.; Alabi, C. A.; Yen, Y.; Heidel, J. D.; Ribas, A. Evidence of RNAi in Humans From Systemically Administered siRNA via Targeted Nanoparticles. *Nature* **2010**, *464*, 1067−1070.

(2) Ivey, K. N.; Muth, A.; Arnold, J.; King, F. W.; Yeh, R.-F.; Fish, J. E.; Hsiao, E. C.; Schwartz, R. J.; Conklin, B. R.; Bernstein, H. S.; Srivastava, D. MicroRNA Regulation of Cell Lineages in Mouse and Human Embryonic Stem Cells. *Cell Stem Cell* **2008**, *2*, 219−229.

(3) Marson, A.; Levine, S. S.; Cole, M. F.; Frampton, G. M.; Brambrink, T.; Johnstone, S.; Guenther, M. G.; Johnston, W. K.; Wernig, M.; Newman, J.; et al. Connecting MicroRNA Genes to the Core Transcriptional Regulatory Circuitry of Embryonic Stem Cells. *Cell* **2008**, *134*, 521−533.

(4) Reynolds, A.; Leake, D.; Boese, Q.; Scaringe, S.; Marshall, W. S.; Khvorova, A. Rational siRNA Design for RNA Interference. *Nat. Biotechnol.* **2004**, *22*, 326−330.

(5) Lu, J.; Getz, G.; Miska, E. A.; Alvarez-Saavedra, E.; Lamb, J.; Peck, D.; Sweet-Cordero, A.; Ebert, B. L.; Mak, R. H.; Ferrando, A. A.; et al. MicroRNA Expression Profiles Classify Human Cancers. *Nature* **2005**, *435*, 834−838.

(6) Volinia, S.; Calin, G. A.; Liu, C.-G.; Ambs, S.; Cimmino, A.; Petrocca, F.; Visone, R.; Iorio, M.; Roldo, C.; Ferracin, M.; et al. A MicroRNA Expression Signature of Human Solid Tumors Defines Cancer Gene Targets. *Proc. Natl. Acad. Sci. U. S. A.* **2006**, *103*, 2257−2261.

(7) Schiffelers, R. M.; Ansari, A.; Xu, J.; Zhou, Q.; Tang, Q.; Storm, G.; Molema, G.; Lu, P. Y.; Scaria, P. V.; Woodle, M. C. Cancer siRNA Therapy by Tumor Selective Delivery With Ligand-Targeted Sterically Stabilized Nanoparticle. *Nucleic Acids Res.* **2004**, *32*, e149−e149.

(8) Turner, J. J.; Jones, S. W.; Moschos, S. A.; Lindsay, M. A.; Gait, M. J. MALDI-TOF Mass Spectral Analysis of siRNA Degradation in Serum Confirms an RNAse A-like Activity. *Mol. BioSyst.* **2007**, *3*, 43−50.

(9) Zhou, J.; Wu, J.; Hafdi, N.; Behr, J.-P.; Erbacher, P.; Peng, L. PAMAM Dendrimers for Efficient siRNA Delivery and Potent Gene Silencing. *Chem. Commun.* **2006**, 2362−2364.

(10) Katas, H.; Alpar, H. O. Development and Characterisation of Chitosan Nanoparticles for siRNA Delivery. *J. Controlled Release* **2006**, *115*, 216−225.

(11) Hurst, S. J.; Lytton-Jean, A. K.; Mirkin, C. A. Maximizing DNA Loading on a Range of Gold Nanoparticle Sizes. *Anal. Chem.* **2006**, *78*, 8313−8318.

(12) Zhang, J.; Malicka, J.; Gryczynski, I.; Lakowicz, J. R. Surface-Enhanced Fluorescence of Fluorescein-Labeled Oligonucleotides Capped on Silver Nanoparticles. *J. Phys. Chem. B* **2005**, *109*, 7643−7648.

(13) Brown, P. K.; Qureshi, A. T.; Moll, A. N.; Hayes, D. J.; Monroe, W. T. Silver Nanoscale Antisense Drug Delivery System for Photoactivated Gene Silencing. *ACS Nano* **2013**, *7*, 2948−2959.

(14) Qureshi, A. T.; Monroe, W. T.; Dasa, V.; Gimble, J. M.; Hayes, D. J. miR-148b−Nanoparticle Conjugates for Light Mediated Osteogenesis of Human Adipose Stromal/Stem Cells. *Biomaterials* **2013**, *34*, 7799−7810.

(15) Braun, G. B.; Pallaoro, A.; Wu, G.; Missirlis, D.; Zasadzinski, J. A.; Tirrell, M.; Reich, N. O. Laser-Activated Gene Silencing via Gold Nanoshell− siRNA Conjugates. *ACS Nano* **2009**, *3*, 2007−2015.

(16) Takahashi, H.; Niidome, Y.; Yamada, S. Controlled Release of Plasmid DNA From Gold Nanorods Induced by Pulsed Near-Infrared Light. *Chem. Commun.* **2005**, 2247−2249.

(17) Vivero-Escoto, J. L.; Slowing, I. I.; Wu, C.-W.; Lin, V. S.-Y. Photoinduced Intracellular Controlled Release Drug Delivery in Human Cells by Gold-Capped Mesoporous Silica Nanosphere. *J. Am. Chem. Soc.* **2009**, *131*, 3462−3463.

(18) Wijaya, A.; Schaffer, S. B.; Pallares, I. G.; Hamad-Schifferli, K. Selective Release of Multiple DNA Oligonucleotides From Gold Nanorods. *ACS Nano* **2009**, *3*, 80−86.

(19) Ghosh, P.; Han, G.; De, M.; Kim, C. K.; Rotello, V. M. Gold Nanoparticles in Delivery Applications. *Adv. Drug Delivery Rev.* **2008**, *60*, 1307−1315.

(20) Chanana, M.; Liz-Marzan, L. M. Coating Matters: the Influence of Coating Materials on the Optical Properties of Gold Nanoparticles. *Nanophotonics* **2012**, *1*, 199−220.

(21) Eustis, S.; El-Sayed, M. A. Why Gold Nanoparticles are More Precious Than Pretty Gold: Noble Metal Surface Plasmon Resonance and its Enhancement of the Radiative and Nonradiative Properties of Nanocrystals of Different Shapes. *Chem. Soc. Rev.* **2006**, *35*, 209−217.

(22) Haber, L. H.; Kwok, S. J. J.; Semeraro, M.; Eisenthal, K. B. Probing the Colloidal Gold Nanoparticle/Aqueous Interface With Second Harmonic Generation. *Chem. Phys. Lett.* **2011**, *507*, 11−14.

(23) Kamat, P. V. Photophysical, Photochemical and Photocatalytic Aspects of Metal Nanoparticles. *J. Phys. Chem. B* **2002**, *106*, 7729−7744.

(24) Qian, X.; Peng, X.-H.; Ansari, D. O.; Yin-Goen, Q.; Chen, G. Z.; Shin, D. M.; Yang, L.; Young, A. N.; Wang, M. D.; Nie, S. In Vivo Tumor Targeting and Spectroscopic Detection With Surface-Enhanced Raman Nanoparticle Tags. *Nat. Biotechnol.* **2007**, *26*, 83−90.

(25) Wustholz, K. L.; Henry, A.-I.; McMahon, J. M.; Freeman, R. G.; Valley, N.; Piotti, M. E.; Natan, M. J.; Schatz, G. C.; Duyne, R. P. V. Structure−Activity Relationships in Gold Nanoparticle Dimers and Trimers for Surface-Enhanced Raman Spectroscopy. *J. Am. Chem. Soc.* **2010**, *132*, 10903−10910.

(26) Bardhan, R.; Grady, N. K.; Cole, J. R.; Joshi, A.; Halas, N. J. Fluorescence Enhancement by Au Nanostructures: Nanoshells and Nanorods. *ACS Nano* **2009**, *3*, 744−752.

(27) Tam, F.; Goodrich, G. P.; Johnson, B. R.; Halas, N. J. Plasmonic Enhancement of Molecular Fluorescence. *Nano Lett.* **2007**, *7*, 496−501.

(28) Karam, T. E.; Haber, L. H. Molecular Adsorption and Resonance Coupling at the Colloidal Gold Nanoparticle Interface. *J. Phys. Chem. C* **2014**, *118*, 642−649.

(29) Dreaden, E. C.; Alkilany, A. M.; Huang, X. H.; Murphy, C. J.; El-Sayed, M. A. The Golden Age: Gold Nanoparticles for Biomedicine. *Chem. Soc. Rev.* **2012**, *41*, 2740−2779.

(30) Oldenburg, S. J.; Averitt, R. D.; Westcott, S. L.; Halas, N. J. Nanoengineering of Optical Resonances. *Chem. Phys. Lett.* **1998**, *288*, 243−247.

(31) Skrabalak, S. E.; Chen, J.; Sun, Y.; Lu, X.; Au, L.; Cobley, C. M.; Xia, Y. Gold Nanocages: Synthesis, Properties, and Applications. *Acc. Chem. Res.* **2008**, *41*, 1587−1595.

(32) Ghosh, P. S.; Kim, C.-K.; Han, G.; Forbes, N. S.; Rotello, V. M. Efficient Gene Delivery Vectors by Tuning the Surface Charge Density of Amino Acid-Functionalized Gold Nanoparticles. *ACS Nano* **2008**, *2*, 2213−2218.

(33) Lee, S. E.; Lee, L. P. Nanoplasmonic Gene Regulation. *Curr. Opin. Chem. Biol.* **2010**, *14*, 623−633.

(34) Eisenthal, K. B. Second Harmonic Spectroscopy of Aqueous Nano-and Microparticle Interfaces. *Chem. Rev.* **2006**, *106*, 1462−1477.

(35) Gonella, G.; Dai, H.-L. Second Harmonic Light Scattering from the Surface of Colloidal Objects: Theory and Applications. *Langmuir* **2014**, *30*, 2588−2599.

(36) Yan, E. C. Y.; Liu, Y.; Eisenthal, K. B. New Method for Determination of Surface Potential of Microscopic Particles by Second Harmonic Generation. *J. Phys. Chem. B* **1998**, *102*, 6331−6336.

(37) Knappenberger, K. L., Jr; Dowgiallo, A.-M.; Chandra, M.; Jarrett, J. W. Probing the Structure−Property Interplay of Plasmonic Nanoparticle Transducers Using Femtosecond Laser Spectroscopy. *J. Phys. Chem. Lett.* **2013**, *4*, 1109−1119.

(38) Doughty, B.; Kazer, S. W.; Eisenthal, K. B. Binding and Cleavage of DNA With the Restriction Enzyme EcoR1 Using Time-Resolved Second Harmonic Generation. *Proc. Natl. Acad. Sci. U. S. A.* **2011**, *108*, 19979−19984.

(39) Malin, J. N.; Holland, J. G.; Saslow, S. A.; Geiger, F. M. U(VI) Adsorption and Speciation at the Acidic Silica/Water Interface Studied

DOI: 10.1021/acs.langmuir.5b02199
Langmuir XXXX, XXX, XXX−XXX

by Resonant and Nonresonant Second Harmonic Generation. *J. Phys. Chem. C* **2011**, *115*, 13353−13360.
(40) Walter, S. R.; Young, K. L.; Holland, J. G.; Gieseck, R. L.; Mirkin, C. A.; Geiger, F. M. Counting the Number of Magnesium Ions Bound to the Surface-Immobilized Thymine Oligonucleotides That Comprise Spherical Nucleic Acids. *J. Am. Chem. Soc.* **2013**, *135*, 17339−17348.
(41) Roke, S.; Gonella, G. Nonlinear Light Scattering and Spectroscopy of Particles and Droplets in Liquids. *Annu. Rev. Phys. Chem.* **2012**, *63*, 353−378.
(42) Gonella, G.; Gan, W.; Xu, B.; Dai, H.-L. The Effect of Composition, Morphology, and Susceptibility on Nonlinear Light Scattering From Metallic and Dielectric Nanoparticles. *J. Phys. Chem. Lett.* **2012**, *3*, 2877−2881.
(43) Doughty, B.; Ma, Y.-Z.; Shaw, R. W. Probing Interfacial Electronic States in CdSe Quantum Dots using Second Harmonic Generation Spectroscopy. *J. Phys. Chem. C* **2015**, *119*, 2752−2760.
(44) Schurer, B.; Wunderlich, S.; Sauerbeck, C.; Peschel, U.; Peukert, W. Probing Colloidal Interfaces by Angle-Resolved Second Harmonic Light Scattering. *Phys. Rev. B: Condens. Matter Mater. Phys.* **2010**, *82*, 241404.
(45) Kumal, R. R.; Karam, T. E.; Haber, L. H. Determination of the Surface Charge Density of Colloidal Gold Nanoparticles Using Second Harmonic Generation. *J. Phys. Chem. C* **2015**, *119*, 16200−16207.
(46) Bai, X.; Li, Z.; Jockusch, S.; Turro, N. J.; Ju, J. Photocleavage of a 2-Nitrobenzyl Linker Bridging a Fluorophore to the 5′ end of DNA. *Proc. Natl. Acad. Sci. U. S. A.* **2003**, *100*, 409−413.
(47) Hiemenz, P. C.; Rajagopalan, R. *Principles of Colloid and Surface Chemistry*, Revised and Expanded, 3rd ed.; CRC Press: New York, 1997.

DOI: 10.1021/acs.langmuir.5b02199
Langmuir XXXX, XXX, XXX−XXX